IEEE Access
Multidisciplinary | Rapid Review | Open Access Journal

Received September 26, 2021, accepted October 3, 2021, date of publication October 13, 2021, date of current version October 26, 2021.

Digital Object Identifier 10.1109/ACCESS.2021.3119614

Improved Deadbeat Predictive Current Control of Permanent Magnet Synchronous Motor Using a Novel Stator Current and Disturbance Observer

ZHENJIE GONG[1], CHENGNING ZHANG[1], XIN BA[1,2], AND YOUGUANG GUO[2], (Senior Member, IEEE)

[1]National Engineering Laboratory for Electric Vehicles, School of Mechanical Engineering, Beijing Institute of Technology, Beijing 100081, China
[2]School of Electrical and Data Engineering, University of Technology Sydney, Ultimo, NSW 2007, Australia

Corresponding author: Xin Ba (xin.ba@bit.edu.cn)

This work was supported in part by key Areas of Guangdong Province under the Project Name: Integration and industrialization of high performance, long endurance and integrated electric drive system (Grant 2019B090910001).

ABSTRACT Thanks to the merits of superior dynamic response capability and current tracking performance, the deadbeat predictive current control (DPCC) has become a research hotspot for the permanent magnet synchronous motor (PMSM) drive system. However, DPCC is a model parameter sensitive control method. If there is a motor parameter mismatch, the performance of the DPCC drive system in terms of expected voltage vector, current harmonics, and torque ripple would be influenced. In this paper, firstly, a novel power sliding mode reaching law is proposed, which shortens the convergence time of the system state no matter what the initial state is. Then, an improved non-homogeneous disturbance observer (NHDO) with the proposed power sliding mode reaching law is established, which guarantees *d-q* axis current errors converge to zero when the PMSM drive system suffers uncertain disturbances, such as motor parameter mismatch. Finally, an improved DPCC using the novel stator current and disturbance observer, which includes the proposed power sliding mode reaching law and NHDO, is established. Hence the accuracy of the predicted current increases significantly, and voltage vectors can be immediately compensated once disturbances occur. Both simulation and platform experiments verify that the improved DPCC can maintain the current tracking performance with lower current ripples than the traditional DPCC when the major motor parameters mismatch. The proposed novel stator current and disturbance observer may also enhance the PMSM's drive performance under other control strategies.

INDEX TERMS Deadbeat predictive current control, disturbance suppression, non-homogeneous disturbance observer, parameter mismatch, stator current and disturbance observer.

I. INTRODUCTION

The performance of the current control strategy has a significant impact on the permanent magnet synchronous motor (PMSM) under different working conditions. Scholars have proposed many control methods to achieve precise and fast current dynamic response control. The commonly used current control algorithms are the proportional-integral (PI) control [1]–[4] and model predictive control (MPC) [5]–[9].

The PI control has been widely used in industrial applications since its high reliability and straightforward structure [10]. However, the PI control cannot meet high accuracy dynamic control requirements, especially when there are internal and external unknown disturbances [11]. The predictive control based on the PMSM mathematical model can acquire better dynamic and steady-state performance [12]. The MPC has two forms: finite set control model predictive control (FSC-MPC) and continuous set control model predictive current control (CSC-MPC) [13]. The FSC-MPC selects one of the six fundamental vectors as the voltage vector for the output by minimizing the cost function. For multi-step prediction, the computational effort of FSC-MPC grows exponentially. In comparison, the CSC-MPC can obtain better static performance with less computation. Deadbeat predictive current control (DPCC), as one of the CSC-MPC, has been widely used for improving the high accuracy dynamic and steady performance of the drive system.

The associate editor coordinating the review of this manuscript and approving it for publication was Shihong Ding.

The accuracy of DPCC is highly dependent on the accuracy of the controlled mathematical model, which means that model parameter mismatch will lead to deviations in prediction calculations. In addition, the control delay of the discrete model will decrease the performance of the controlled system [14]. Reference [15] analyzed seven main parameter identification methods to reduce the influence caused by parameter mismatch of PMSM.

Furthermore, scholars have proposed a number of control strategies combined with disturbance observers to improve the accuracy of predictive control performance [5], [16]–[20]. Reference [5] proposed a novel super-twisting algorithm observer by designing an adjustable gain that changes the system state to realize parameter error estimation. Reference [16] developed an extended state observer (ESO) to observe the stator current when parameter mismatch in the open-winding PMSM with a common DC bus. Reference [17] proposed a predictive speed control based on the continuous control and the fast terminal cost index to enhance the tracking performance. Reference [18] proposed a model predictive torque control based on active disturbance rejection to solve the unavoidable electromagnetic torque tracking error caused by parameter mismatch. Reference [19] designed a discrete-time power disturbance observer to predict the complex state and observe unknown disturbances of the controlled system as set-total disturbances. Reference [20] used a disturbance observer to improve the robustness under parameter mismatch conditions, and analyzed the internal relationship between the accuracy of the discrete control set and the disturbance observer.

A stator current disturbance observer was designed in [21]. When the motor parameters mismatch, the observer can predict the future current and perform state deviation compensation accurately. The robustness of the observer ensures the stability of the drive system under random disturbances [22], [23]. To enhance the stability of the system, the disturbance observer adopts the exponential sliding mode reaching law which does not require the high modeling accuracy of the controlled system. Sliding mode control (SMC) is invariant to the matching disturbance items in the system during the sliding mode motion stage [24], [25]. Therefore, it can use SMC characteristics to solve the parameter sensitivity problem of predictive control. No matter what switching gain is selected in the SMC, it will cause the contradiction between convergence speed and chattering irreconcilable. There are two main reasons for the chattering: (1) there is a parasitic dynamic in series with the control system, which causes a small high-frequency oscillation; and (2) non-ideal switching characteristics cause high-frequency oscillations.

Scholars have proposed many methods to suppress the chattering problem [26]–[31]. In [26], an adaptive SMC was developed to accelerate the convergence in a limited time and reduce the chattering phenomenon of the system state on the sliding surface. Reference [27] designed a type of non-linear fractional-order PID sliding surface combined with the adaptive super-twisting reaching law for speed control of the PMSM. The sliding mode stage can ensure a fast convergence rate, good robustness, and reduced chattering. Reference [28] proposed an adaptive SMC method combined with a disturbance torque observer to suppress chattering, and this observer can optimize the speed tracking performance of the PMSM. Reference [29] presented a novel SMC algorithm that can shorten the convergence time. To improve the anti-disturbance capability of the PMSM, [30] proposed an ESO based on the fast terminal sliding mode control method, which can enhance immunity to load disturbances, converge in a limited time, and effectively suppress chattering. Reference [31] proposed an SMC method with fuzzy switching gain to eliminate the chattering phenomenon by using the saturation function.

The main novel contributions of this study are as follows: firstly, a faster power sliding mode reaching law is developed to promote the dynamic response of the PMSM drive system when disturbances occur. Secondly, an improved non-homogeneous disturbance observer (NHDO) enables the PMSM drive system to reach a stable state in a finite time. Thirdly, an improved DPCC with the novel stator current and disturbance observer, which incorporates the proposed power sliding mode reaching law and NHDO, is established, and the robustness of the drive system has been boosted when there exists motor parameter mismatch.

The paper is structured as follows: Section II establishes the conventional DPCC of PMSM. Section III proposes the derivation process of piecewise sliding mode control and carries out the fixed-time stability analysis. The DPCC with a novel SCDO of PMSM is illustrated in Section IV. An improved DPCC, which has combined an NHDO to observe and eliminate state error bound caused by disturbance, is presented in Section V. Sections VI and VII validate the effectiveness and reliability of the proposed control method through simulations and experiments. Section VIII gives the conclusion and some vital discussion.

II. DEADBEAT PREDICTIVE CURRENT CONTROL OF PMSM

A. MATHEMATICAL MODELS OF PMSM

Assume that the PMSM stator windings are Y-connected, and the three-phase windings are symmetrically distributed. Ignore the core loss and non-linear magnetic characteristics of the stator core. The voltage equations of the PMSM in a synchronous rotating coordinate system can be expressed as:

$$\begin{cases} u_{\mathrm{d}} = R_{\mathrm{s}} i_{\mathrm{d}} + L_{\mathrm{d}} \dfrac{\mathrm{d}i_{\mathrm{d}}}{\mathrm{d}t} - \omega_{\mathrm{e}} L_{\mathrm{q}} i_{\mathrm{q}} \\ u_{\mathrm{q}} = R_{\mathrm{s}} i_{\mathrm{q}} + L_{\mathrm{q}} \dfrac{\mathrm{d}i_{\mathrm{q}}}{\mathrm{d}t} + \omega_{\mathrm{e}} L_{\mathrm{d}} i_{\mathrm{d}} + \psi_{\mathrm{f}} \omega_{\mathrm{e}} \end{cases} \tag{1}$$

where u_{d} and u_{q} are the d- and q-axis stator voltages, i_{d} and i_{q} are the d- and q-axis currents, L_{d} and L_{q} are the d- and q-axis inductance, R_{s} is the stator resistance, Ψ_{f} is the flux linkage of permanent magnets, and ω_{e} is the angular velocity.

B. DISCRETE-TIME MATHEMATICAL MODEL FOR DPCC

Assume that the control system sampling time T_s is short enough, and in the surface-mounted PMSM (SPMSM), $L_d = L_q = L$. The SPMSM discretization is

$$\boldsymbol{i}(k+1) = \boldsymbol{A}(k)\boldsymbol{i}(k) + \boldsymbol{C}\boldsymbol{u}(k) + \boldsymbol{D}(k) \tag{2}$$

where

$$\boldsymbol{i}(k+1) = \begin{bmatrix} i_d(k+1) \\ i_q(k+1) \end{bmatrix}, \quad \boldsymbol{i}(k) = \begin{bmatrix} i_d(k) \\ i_q(k) \end{bmatrix},$$
$$\boldsymbol{u}(k) = \begin{bmatrix} u_d(k) \\ u_q(k) \end{bmatrix},$$
$$\boldsymbol{A}(k) = \begin{bmatrix} 1 - \frac{R_s}{L}T_s & \omega_e T_s \\ -\omega_e T_s & 1 - \frac{R_s}{L}T_s \end{bmatrix}, \quad \boldsymbol{C} = \begin{bmatrix} \frac{T_s}{L} & 0 \\ 0 & \frac{T_s}{L} \end{bmatrix},$$
$$\boldsymbol{D}(k) = \begin{bmatrix} 0 \\ -\frac{\psi_f}{L}T_s\omega_e(k) \end{bmatrix}.$$

In the conventional DPCC method, the output voltage vector equation is:

$$\boldsymbol{u}(k) = \boldsymbol{C}^{-1}(\boldsymbol{i}^*(k+1) - \boldsymbol{A}(k)\boldsymbol{i}(k) - \boldsymbol{D}(k)) \tag{3}$$

where $\boldsymbol{i}^*(k+1) = \begin{bmatrix} i_d^*(k+1) \\ i_q^*(k+1) \end{bmatrix}$ is the reference current matrix.

III. DESIGN OF PIECEWISE POWER SLIDING MODE REACHING LAW

A. COMPARISION OF TWO DIFFERENT REACHING LAWS

Gao presented the concept of reaching law and analyzed isokinetic reaching law, exponential reaching law, and power reaching law [32]. Among them, the isokinetic reaching law has a constant reaching rate, and the exponential reaching law adds a linear term to reduce convergence time. However, both of them contain a fixed gain of the *sign* function, and there are constantly chattering. The gain of the sign function of the power reaching law is variable power gain and reduces the amplitude of chattering at the balance point. Therefore, [33] analyzed that both fast power sliding mode reaching law (FPSMRL) and dual power sliding mode reaching law (DPSMRL) have second-order slip model properties.

The FPSMRL and DPSMRL can be respectively expressed as:

$$\dot{s} = -k_1 s - k_2 |s|^{1-\gamma} \operatorname{sgn}(s) \tag{4}$$
$$\dot{s} = -k_1 |s|^{1+\gamma} \operatorname{sgn}(s) - k_2 |s|^{1-\gamma} \operatorname{sgn}(s) \tag{5}$$

where $k_1 > 0$ and $k_2 > 0$ are the designed constants, and γ is a positive power series that satisfy the condition $0 < \gamma < 1$. Those above-mentioned two laws can realize the second-order sliding mode characteristics, i.e., make $s = \dot{s} = 0$ in a finite time without considering the disturbance. The system state arriving at the sliding mode surface from the initial state can be discussed in two stages: (a) $|s| > 1$: $-k_1 s$ in (4) and $-k_1|s|^{1+\gamma}\operatorname{sgn}(s)$ in (5) play the dominant role; (b) $|s| \le 1$: $-k_2|s|^{1-\gamma}\operatorname{sgn}(s)$ in (4) and (5) play the dominant role.

Assume that the initial state is $s(0) = |s_0| > 1$. The convergence times of the two laws are discussed, respectively.

1) THE FIRST STAGE: $|s(0)| = s_0 \rightarrow |s(t_1)| = 1$

Considering $-k_2|s|^{1-\gamma}\operatorname{sgn}(s)$ does not play a dominant role, (4) and (5) can be simplified as:

$$\dot{s} = -k_1 s \tag{6}$$
$$\dot{s} = -k_1 |s|^{1+\gamma} \operatorname{sgn}(s) \tag{7}$$

The integration of (6) and (7) can be calculated as:

$$s(t_{f1}) = s(0)\exp(-k_1 t_{f1}) \tag{8}$$
$$s^{-\gamma}(t_{d1}) = s^{-\gamma}(0) - (-\gamma)k_1 t_{d1} \tag{9}$$

where t_{f1} and t_{d1} denote the times required for the state $s(0)$ to converge to the sliding surface $s = 1$ under FPSMRL and DPSMRL, respectively.

The convergence time of the first stage is as follows:

$$t_{f1} = \frac{1}{k_1}\ln(s(0)) \tag{10}$$
$$t_{d1} = \frac{1 - s^{-\gamma}(0)}{k_1 \alpha} \tag{11}$$

Comparing (10) and (11), we have $t_{f1} > t_{d1}$. The DPSMRL has a faster convergence rate than the FPSMRL in the first stage under the same conditions.

2) THE SECOND STAGE: $|s(t_1)| = 1 \rightarrow |s(t_2)| = 0$

$-k_2|s|^{1-\gamma}\operatorname{sgn}(s)$ plays a dominant role in both (4) and (5). Therefore, all the items should be considered in this convergence time of this stage.

The convergence time for the system state from any initial state s_0 to origin T_f in (4) can be calculated as [34]:

$$T_f = \frac{1}{k_1\gamma}\ln\left(1 + \frac{k_1}{k_2}|s_0|^{\gamma}\right) \tag{12}$$

Similarly, the convergence time for the system state from any initial state s_0 to origin T_d in (5) can be calculated as [35]:

$$T_d = \int_0^{|s_0|} \frac{1}{k_1 x^{1+\gamma} + k_2 x^{1-\gamma}} \mathrm{d}s = \frac{|s_0|^{-\gamma}}{-\gamma} k_1^{-\frac{\gamma}{1+\gamma}} F\left(1, \frac{1}{2}; \frac{3}{2}; -\frac{k_2}{k_1}|s_0|^{-2\gamma}\right) \tag{13}$$

where $F(\bullet)$ denotes the Gauss' hypergeometric function [36].

Substituting the second stage initial state $|s_0| = |s(t_1)| = 1$ into (12) and (13) yields:

$$t_{f2} = T_f\big|_{s_0=1} = \frac{1}{k_1\gamma}\ln\left(1 + \frac{k_1}{k_2}\right) \tag{14}$$

$$t_{d2} = T_d\big|_{s_0=1} = \frac{k_1^{-\frac{\gamma}{1+\gamma}}}{-\gamma} F\left(1, \frac{1}{2}; \frac{3}{2}; -\frac{k_2}{k_1}\right) \tag{15}$$

where t_{f2} and t_{d2} respectively denote the convergence time for the system state from the sliding surface $s = 1$ to $s = 0$ in FPSMRL and DPSMRL.

Through the Gauss' hypergeometric function and the power series expansion of arctan (•), the quotient of (14) and (15) can be written as [37]:

$$\frac{t_{d2}}{t_{f2}} = \frac{\sqrt{k_1/k_2}\arctan\left(\sqrt{k_1/k_2}\right)}{\ln(1+k_1/k_2)} > 1 \tag{16}$$

It is clear that t_{d2} is greater than t_{f2}. Therefore, the FPSMRL has a faster convergence rate than the DPSMRL in the second stage under the same conditions.

B. A NOVEL POWER SLIDING MODE REACHING LAW

The above-mentioned analysis shows that (4) and (5) have different convergence times at two stages. Therefore, to acquire a fast convergence rate at both of two stages, a piecewise reaching law formula consisting of FPSMRL and DPSMRL is:

$$\dot{s} = -k_1 fal(s, 1+\gamma, \delta) - k_2 |s|^{1-\gamma} \operatorname{sgn}(s) \tag{17}$$

where $k_1 > 0$ and $k_2 > 0$ are the designed constants, and γ is a positive power series which satisfy the condition $0 < \gamma < 1$, $\delta = 1$. Nonlinear piecewise function *fal* (•) is:

$$fal(s, 1+\gamma, \delta) = \begin{cases} |s|^{1+\gamma}\operatorname{sgn}(s), & |s| > \delta \\ \dfrac{s}{\delta^{-\gamma}}, & |s| \le \delta \end{cases} \tag{18}$$

When the phase trajectory line is away from the sliding mode surface, i.e., $|s| > 1$, (17) is equivalent to (5). When $|s| \le 1$, (17) is equivalent to (4).

C. FIXED-TIME STABILITY ANALYSIS

Define an initial state of the system as $x_0 \in \mathbb{R}^n$. The origin is the global finite-time convergence equilibrium point. If the convergence time function $T(x_0)$ is bounded, $T(x_0) \le T_{\max}$ for any $x_0 \in \mathbb{R}^n$ is established. Then the origin is the global fixed-time convergence equilibrium of the system. Since the convergence time is independent of the initial state of the system and only related to the constant parameters of the system, the fixed-time stability analysis is adopted in this study. Define a continuous radial unbounded function V: $\mathbb{R}^n \to \mathbb{R}$, an open connected set Ω: $0 \in \text{int}(\Omega)$. For $\mu \in (0,1)$, $\nu \in \mathbb{R}$, $r_\mu \in \mathbb{R}_+$, $r_\nu \in \mathbb{R}_+$:

$$\dot{V}(x) \le \begin{cases} -r_\mu V^{1-\mu}(x), & x \in \Omega : V(x) \le 1 \\ -r_\nu V^{1+\nu}(x), & x \in \Omega : V(x) > 1 \end{cases} \quad t > t_0, x \in \Omega \tag{19}$$

Then the origin of the system is a fixed-time stable point. The maximum convergence time is estimated by:

$$T_x \le T_{\max} \le \frac{1}{\mu r_\mu} + \frac{1}{\nu r_\nu} \tag{20}$$

If V is radially unbounded, the origin of the system is a globally fixed-time stable point.

Consider the Lyapunov function as:

$$V = \frac{1}{2}s^2 \tag{21}$$

The derivative of V along the trajectory of (17) is:

$$\begin{aligned} \dot{V} &= s\dot{s} \\ &= \begin{cases} -k_1 V - k_2 V^{1-\frac{\gamma}{2}}, & V \le 1 \\ -k_1 V^{1+\frac{\gamma}{2}} - k_2 V^{1-\frac{\gamma}{2}}, & V > 1 \end{cases} \\ &\le \begin{cases} -k_2 V^{1-\frac{\gamma}{2}}, & V \le 1 \\ -k_1 V^{1+\frac{\gamma}{2}}, & V > 1 \end{cases} \end{aligned} \tag{22}$$

where $r_\mu = k_2$, $r_\nu = k_1$, and $\mu = \nu = \gamma/2$. The convergence time T satisfies the following inequality:

$$T \le T_{\max} \le \frac{1}{\mu r_\mu} + \frac{1}{\nu r_\nu} = \frac{1}{\gamma}\left(\frac{1}{k_2} + \frac{1}{k_1}\right) \tag{23}$$

IV. DEADBEAT PREDICTIVE CURRENT CONTROL METHOD WITH STATOR CURRENT AND DISTURBANCE OBSERVER (DPCC+SCDO)

A. PROPOSED STATOR CURRENT AND DISTURBANCE OBSERVER

Since the parameter mismatch is the most common disturbance, the drive system performances under the parameter mismatch are studied in the following sections. With the parameter mismatch, the extended voltage dynamic equations of the SPMSM can be written as:

$$\begin{cases} u_\mathrm{d} = R_\mathrm{s} i_\mathrm{d} + L\dfrac{di_\mathrm{d}}{dt} - \omega_\mathrm{e} L i_\mathrm{q} + \Gamma_\mathrm{d} \\ u_\mathrm{q} = R_\mathrm{s} i_\mathrm{q} + L\dfrac{di_\mathrm{q}}{dt} + \omega_\mathrm{e} L i_\mathrm{d} + \psi_\mathrm{f}\omega_\mathrm{e} + \Gamma_\mathrm{q} \end{cases} \tag{24}$$

$$\begin{cases} \Gamma_\mathrm{d} = \Delta R_\mathrm{s} i_\mathrm{d} + \Delta L\dfrac{di_\mathrm{d}}{dt} - \omega_\mathrm{e}\Delta L i_\mathrm{q} \\ \Gamma_\mathrm{q} = \Delta R_\mathrm{s} i_\mathrm{q} + \Delta L\dfrac{di_\mathrm{q}}{dt} + \omega_\mathrm{e}\Delta L i_\mathrm{d} + \Delta\psi_\mathrm{f}\omega_\mathrm{e} \end{cases} \tag{25}$$

where $L_\mathrm{d} = L_\mathrm{q} = L$ in this SPMSM. Γ_d and Γ_q respectively represent the d- and q-axis collective parameter disturbances, including the voltage change caused by resistance variation ΔR_s, inductance variation ΔL, and permanent magnetic flux linkage variation $\Delta\Psi_\mathrm{f}$.

To estimate the voltage change caused by parameter change, (24) can be redesigned as:

$$\begin{cases} u_\mathrm{d} = R_\mathrm{s}\hat{i}_\mathrm{d} + L\dot{\hat{i}}_\mathrm{d} - \omega_\mathrm{e} L i_\mathrm{q} + \hat{\Gamma}_\mathrm{d} + u_\mathrm{d\_SMC} \\ u_\mathrm{q} = R_\mathrm{s}\hat{i}_\mathrm{q} + L\dot{\hat{i}}_\mathrm{q} + \omega_\mathrm{e} L i_\mathrm{d} + \psi_\mathrm{f}\omega_\mathrm{e} + \hat{\Gamma}_\mathrm{q} + u_\mathrm{q\_SMC} \end{cases} \tag{26}$$

$$\begin{cases} \dfrac{d\hat{\Gamma}_\mathrm{d}}{dt} = u_\mathrm{d\_SMC} \\ \dfrac{d\hat{\Gamma}_\mathrm{q}}{dt} = u_\mathrm{q\_SMC} \end{cases} \tag{27}$$

where $\hat{\Gamma}_\mathrm{d}$ and $\hat{\Gamma}_\mathrm{q}$ are the estimations of Γ_d and Γ_q, $\hat{i}_\mathrm{d}$ and $\hat{i}_\mathrm{q}$ the estimations of d- and q-axis currents, and $u_\mathrm{d\_SMC}$ and $u_\mathrm{q\_SMC}$ are the d- and q-axis PPSMRL functions, respectively.

According to (24) and (26), the current error state equation between the actual model and predicted model can be obtained as:

$$\begin{cases} \dot{e}_\mathrm{d} = -\dfrac{R_\mathrm{s}}{L}e_\mathrm{d} - \dfrac{1}{L}(\Gamma_\mathrm{d} - \hat{\Gamma}_\mathrm{d}) + \dfrac{1}{L}u_\mathrm{d\_SMC} \\ \dot{e}_\mathrm{q} = -\dfrac{R_\mathrm{s}}{L}e_\mathrm{q} - \dfrac{1}{L}(\Gamma_\mathrm{q} - \hat{\Gamma}_\mathrm{q}) + \dfrac{1}{L}u_\mathrm{q\_SMC} \end{cases} \tag{28}$$

$$\begin{cases} e_{\mathrm{d}} = i_{\mathrm{d}} - \hat{i}_{\mathrm{d}} \\ e_{\mathrm{q}} = i_{\mathrm{q}} - \hat{i}_{\mathrm{q}} \end{cases} \tag{29}$$

where e_{d} and e_{q} are the d- and q-axis current estimation errors, respectively.

According to the proposed PPSMRL in Section III, the novel sliding mode functions $u_{\mathrm{d\_SMC}}$ and $u_{\mathrm{q\_SMC}}$ are designed. First, the sliding mode surface is designed as a linear sliding mode surface, $s_{\mathrm{d,q}} = e_{\mathrm{d,q}} = i_{\mathrm{d,q}} - \hat{i}_{\mathrm{d,q}}$. Second, the PPSMRL is selected as the sliding mode reaching law.

$$\begin{cases} \dot{s}_{\mathrm{d}} = -k_1 fal(s_{\mathrm{d}}, 1+\gamma, \delta) - k_2 \left|s_{\mathrm{d}}\right|^{1-\gamma} \mathrm{sgn}(s_{\mathrm{d}}) \\ \dot{s}_{\mathrm{q}} = -k_1 fal(s_{\mathrm{q}}, 1+\gamma, \delta) - k_2 \left|s_{\mathrm{q}}\right|^{1-\gamma} \mathrm{sgn}(s_{\mathrm{q}}) \end{cases} \tag{30}$$

$$\begin{cases} fal(s_{\mathrm{d}}, 1+\gamma, \delta) = \begin{cases} \left|s_{\mathrm{d}}\right|^{1+\gamma} \mathrm{sgn}(s_{\mathrm{d}}), & \left|s_{\mathrm{d}}\right| > \delta \\ \dfrac{s_{\mathrm{d}}}{\delta^{-\gamma}}, & \left|s_{\mathrm{d}}\right| \le \delta \end{cases} \\ fal(s_{\mathrm{q}}, 1+\gamma, \delta) = \begin{cases} \left|s_{\mathrm{q}}\right|^{1+\gamma} \mathrm{sgn}(s_{\mathrm{q}}), & \left|s_{\mathrm{q}}\right| > \delta \\ \dfrac{s_{\mathrm{q}}}{\delta^{-\gamma}}, & \left|s_{\mathrm{q}}\right| \le \delta \end{cases} \end{cases} \tag{31}$$

Substituting (28) into (30) yields:

$$\begin{cases} -\dfrac{R_{\mathrm{s}}}{L} e_{\mathrm{d}} - \dfrac{1}{L}(\Gamma_{\mathrm{d}} - \hat{\Gamma}_{\mathrm{d}}) + \dfrac{1}{L} u_{\mathrm{d\_SMC}} \\ \qquad = -k_1 fal(e_{\mathrm{d}}, 1+\gamma, \delta) - k_2 \left|e_{\mathrm{d}}\right|^{1-\gamma} \mathrm{sgn}(e_{\mathrm{d}}) \\ -\dfrac{R_{\mathrm{s}}}{L} e_{\mathrm{q}} - \dfrac{1}{L}(\Gamma_{\mathrm{q}} - \hat{\Gamma}_{\mathrm{q}}) + \dfrac{1}{L} u_{\mathrm{q\_SMC}} \\ \qquad = -k_1 fal(e_{\mathrm{q}}, 1+\gamma, \delta) - k_2 \left|e_{\mathrm{q}}\right|^{1-\gamma} \mathrm{sgn}(e_{\mathrm{q}}) \end{cases} \tag{32}$$

Considering $\Gamma_{\mathrm{d}} - \hat{\Gamma}_{\mathrm{d}}$ and $\Gamma_{\mathrm{q}} - \hat{\Gamma}_{\mathrm{q}}$ as the disturbances function, (32) can be simplified as:

$$\begin{cases} u_{\mathrm{d\_SMC}} = -k_1 L fal(e_{\mathrm{d}}, 1+\gamma, \delta) - k_2 L \left|e_{\mathrm{d}}\right|^{1-\gamma} \mathrm{sgn}(e_{\mathrm{d}}) \\ \qquad\qquad + R_{\mathrm{s}} L e_{\mathrm{d}} \\ u_{\mathrm{q\_SMC}} = -k_1 L fal(e_{\mathrm{q}}, 1+\gamma, \delta) - k_2 L \left|e_{\mathrm{q}}\right|^{1-\gamma} \mathrm{sgn}(e_{\mathrm{q}}) \\ \qquad\qquad + R_{\mathrm{s}} L e_{\mathrm{q}} \end{cases} \tag{33}$$

B. ANALYSIS OF STEADY-STATE ERROR BOUNDARY

Take the d-axis as an example. Choosing the Lyapunov function, one has

$$V_{\mathrm{d}} = \frac{1}{2} s_{\mathrm{d}}^2 \tag{34}$$

The derivative of V_{d} can be obtained as:

$$\begin{aligned} \dot{V}_{\mathrm{d}} &= s_{\mathrm{d}} \dot{s}_{\mathrm{d}} \\ &= e_{\mathrm{d}} \dot{e}_{\mathrm{d}} \\ &= -k_1 e_{\mathrm{d}} fal(e_{\mathrm{d}}, 1+\gamma, 1) - k_2 \left|e_{\mathrm{d}}\right|^{2-\gamma} \mathrm{sgn}(e_{\mathrm{d}}) + e_{\mathrm{d}} d_{\mathrm{d}}(t) \end{aligned} \tag{35}$$

Uncertain disturbance about d-axis current estimation errors and d-axis disturbance estimation errors are bounded:

$$\left|d_{\mathrm{d}}(\mathrm{t})\right| \le \mathrm{D_d} \tag{36}$$

where $\mathrm{D_d}$ represents the bound of d-axis uncertain perturbation d_{d}.

Therefore, (35) can be written as follows:

$$\begin{cases} \dot{V}_{\mathrm{d}} = -k_1 \left|e_{\mathrm{d}}\right|^{2+\gamma} - k_2 \left|e_{\mathrm{d}}\right|^{2-\gamma} + d_{\mathrm{d}}(t) \left|e_{\mathrm{d}}\right|, & \left|e_{\mathrm{d}}\right| > 1 \\ \dot{V}_{\mathrm{d}} = -k_1 \left|e_{\mathrm{d}}\right|^{2} - k_2 \left|e_{\mathrm{d}}\right|^{2-\gamma} + d_{\mathrm{d}}(t) \left|e_{\mathrm{d}}\right|, & \left|e_{\mathrm{d}}\right| \le 1 \end{cases} \tag{37}$$

Equation (37) can be expanded into four different forms:

$$\begin{cases} \dot{V}_{\mathrm{d}} \le -k_1 \left|e_{\mathrm{d}}\right|^{2+\gamma} - \left|e_{\mathrm{d}}\right| (k_2 \left|e_{\mathrm{d}}\right|^{1-\gamma} - D_{\mathrm{d}}), & \left|e_{\mathrm{d}}\right| > 1 \\ \dot{V}_{\mathrm{d}} \le -k_2 \left|e_{\mathrm{d}}\right|^{2-\gamma} - \left|e_{\mathrm{d}}\right| (k_1 \left|e_{\mathrm{d}}\right|^{1+\gamma} - D_{\mathrm{d}}), & \left|e_{\mathrm{d}}\right| > 1 \\ \dot{V}_{\mathrm{d}} \le -k_1 \left|e_{\mathrm{d}}\right|^{2} - \left|e_{\mathrm{d}}\right| (k_2 \left|e_{\mathrm{d}}\right|^{1-\gamma} - D_{\mathrm{d}}), & \left|e_{\mathrm{d}}\right| \le 1 \\ \dot{V}_{\mathrm{d}} \le -k_2 \left|e_{\mathrm{d}}\right|^{2-\gamma} - \left|e_{\mathrm{d}}\right| (k_1 \left|e_{\mathrm{d}}\right| - D_{\mathrm{d}}), & \left|e_{\mathrm{d}}\right| \le 1 \end{cases} \tag{38}$$

To satisfy the stability of Lyapunov, k_1 and k_2 are shown in the following table.

TABLE 1. Values of k_1 and k_2 and state error boundary.

Derivative of V_{d}	k_1 or k_2	Error boundary
$\dot{V}_{\mathrm{d}} \le -k_1 \left\|e_{\mathrm{d}}\right\|^{2+\gamma} \le 0$	$k_2 > \dfrac{D_{\mathrm{d}}}{\left\|e_{\mathrm{d}}\right\|^{1-\gamma}}$	$\left\|e_{\mathrm{d}}\right\| < \left(\dfrac{D_{\mathrm{d}}}{k_2}\right)^{\frac{1}{1-\gamma}}$
$\dot{V}_{\mathrm{d}} \le -k_2 \left\|e_{\mathrm{d}}\right\|^{2-\gamma} \le 0$	$k_1 > \dfrac{D_{\mathrm{d}}}{\left\|e_{\mathrm{d}}\right\|^{1+\gamma}}$	$\left\|e_{\mathrm{d}}\right\| < \left(\dfrac{D_{\mathrm{d}}}{k_1}\right)^{\frac{1}{1+\gamma}}$
$\dot{V}_{\mathrm{d}} \le -k_1 \left\|e_{\mathrm{d}}\right\|^{2} \le 0$	$k_2 > \dfrac{D_{\mathrm{d}}}{\left\|e_{\mathrm{d}}\right\|^{1-\gamma}}$	$\left\|e_{\mathrm{d}}\right\| < \left(\dfrac{D_{\mathrm{d}}}{k_2}\right)^{\frac{1}{1-\gamma}}$
$\dot{V}_{\mathrm{d}} \le -k_2 \left\|e_{\mathrm{d}}\right\|^{2-\gamma} \le 0$	$k_1 > \dfrac{D_{\mathrm{d}}}{\left\|e_{\mathrm{d}}\right\|}$	$\left\|e_{\mathrm{d}}\right\| < \left(\dfrac{D_{\mathrm{d}}}{k_1}\right)$

From what has been discussed above, the error e_{d} will reach the boundary shown in Table 1 within the validity period:

$$\left|e_{\mathrm{d}}\right| \le \min\left\{ \left(D_{\mathrm{d}}/k_1\right), \left(D_{\mathrm{d}}/k_1\right)^{1/(1+\gamma)}, \left(D_{\mathrm{d}}/k_2\right)^{1/(1-\gamma)} \right\} \tag{39}$$

To ensure $\dot{V}_{\mathrm{d}} \le 0$, k_1 and k_2 should be selected as:

$$\begin{cases} k_1 > D_{\mathrm{d}} / \left|e_{\mathrm{d}}\right|^{1+\gamma} \\ k_2 > D_{\mathrm{d}} / \left|e_{\mathrm{d}}\right|^{1-\gamma} \end{cases} \tag{40}$$

Similarly, to ensure $\dot{V}_{\mathrm{q}} \le 0$, k_1 and k_2 should be selected as:

$$\begin{cases} k_1 > D_{\mathrm{q}} / \left|e_{\mathrm{q}}\right|^{1+\gamma} \\ k_2 > D_{\mathrm{q}} / \left|e_{\mathrm{q}}\right|^{1-\gamma} \end{cases} \tag{41}$$

To ensure that the whole observer is stable, k_1 and k_2 should be selected as:

$$\begin{cases} k_1 > \max(D_{\mathrm{d}} / \left|e_{\mathrm{d}}\right|^{1+\gamma}, D_{\mathrm{q}} / \left|e_{\mathrm{q}}\right|^{1+\gamma}) \\ k_2 > \max(D_{\mathrm{d}} / \left|e_{\mathrm{d}}\right|^{1-\gamma}, D_{\mathrm{q}} / \left|e_{\mathrm{q}}\right|^{1-\gamma}) \end{cases} \tag{42}$$

where D_{d} and D_{q} represent the bounds of the d-axis and q-axis with uncertain disturbance, respectively.

C. DISCRETE EXPRESSION OF DPCC+SCDO

For the discrete system, if the sampling period T is short enough, at the kth period, the discrete expression form of DPCC+SCDO can be written as:

$$\begin{cases} \boldsymbol{i}(\mathrm{k}+1) = \boldsymbol{A}(\mathrm{k})\boldsymbol{i}(\mathrm{k}) + \boldsymbol{C}\boldsymbol{u}(\mathrm{k}) + \boldsymbol{D}(\mathrm{k}) - \dfrac{T}{L}\hat{\boldsymbol{\Gamma}}(\mathrm{k}) \\ \qquad\qquad -\dfrac{T}{L}\boldsymbol{H}(\mathrm{k}) \\ \boldsymbol{u}(\mathrm{k}+1) = \boldsymbol{C}^{-1}\left[\boldsymbol{i}(\mathrm{k}+2) - \boldsymbol{A}(\mathrm{k})\boldsymbol{i}(\mathrm{k}+1) - \boldsymbol{D}(\mathrm{k}+1)\right] \\ \hat{\boldsymbol{\Gamma}}(\mathrm{k}+1) = \hat{\boldsymbol{\Gamma}}(\mathrm{k}) - T\boldsymbol{H}(\mathrm{k}) \\ \boldsymbol{U}^* = \boldsymbol{u}(\mathrm{k}) + \hat{\boldsymbol{\Gamma}}(\mathrm{k}+1) \end{cases} \tag{43}$$

where

$$\hat{\boldsymbol{\Gamma}}(\mathrm{k}) = \begin{bmatrix} \hat{\Gamma}_{\mathrm{d}}(\mathrm{k}) \\ \hat{\Gamma}_{\mathrm{q}}(\mathrm{k}) \end{bmatrix}, \quad \hat{\boldsymbol{\Gamma}}(\mathrm{k}+1) = \begin{bmatrix} \hat{\Gamma}_{\mathrm{d}}(\mathrm{k}+1) \\ \hat{\Gamma}_{\mathrm{q}}(\mathrm{k}+1) \end{bmatrix},$$
$$\boldsymbol{H}(\mathrm{k}) = \begin{bmatrix} u_{\mathrm{d\_SMC}}(\mathrm{k}) \\ u_{\mathrm{q\_SMC}}(\mathrm{k}) \end{bmatrix}, \quad \boldsymbol{i}(\mathrm{k}+2) = \begin{bmatrix} i_{\mathrm{d}}(\mathrm{k}+2) \\ i_{\mathrm{q}}(\mathrm{k}+2) \end{bmatrix}$$
$$= \begin{bmatrix} i_{\mathrm{d}}^* \\ i_{\mathrm{q}}^* \end{bmatrix},$$
$$\boldsymbol{u}(\mathrm{k}+1) = \begin{bmatrix} u(\mathrm{k}+1) \\ u(\mathrm{k}+1) \end{bmatrix}, \quad \text{and } \boldsymbol{U}^* = \begin{bmatrix} U_d^* \\ U_q^* \end{bmatrix}$$

is the reference voltage of SVPWM.

V. IMPROVED DEADBEAT PREDICTIVE CURRENT CONTROL (DPCC+SCDO+NHDO)

A. ANALYSIS OF THE PIECEWISE POWER SLIDING MODEL REACHING LAW

For the system (17), if $k_1 > 0, k_2 > 0, 0 < \gamma < 1$, then the system state s and $\dot{s}$ tend to 0 in a finite time T.

From (39), when there is uncertainty in the system, the PPSMRL cannot guarantee that s and $\dot{s}$ converge to (0,0) but can only converge to a neighborhood of (0,0) in the limited time.

Consider the following nonlinear system:

$$\dot{s} = -k_1 fal(s, 1+\gamma, 1) - k_2 |s|^{1-\gamma} \operatorname{sgn}(s) + d(t) \tag{44}$$

Assuming the disturbance $d(\mathrm{t}) \neq 0$ and $|d(\mathrm{t})| < D$, D is a positive series which satisfies the condition $D > 0$, s and $\dot{s}$ converge to the following bounds in T.

$$\begin{cases} |s| \le \min\left\{(D/k_1), (D/k_1)^{1/(1+\gamma)}, (D/k_2)^{1/(1-\gamma)}\right\} \\ |\dot{s}| \le \min\left\{\begin{array}{l} fal\left((D), 1+\gamma, 1\right), \\ fal\left((D)^{1/(1+\gamma)} k_1^{\gamma/(1+\gamma)}, 1+\gamma, 1\right), \\ k_1 fal\left((D/k_2)^{1/(1-\gamma)}, 1+\gamma, 1\right) \end{array}\right\} \\ +\min\left\{k_2 (D/k_1)^{1-\gamma}, k_2 (D/k_1)^{(1-\gamma)/(1+\gamma)}, (D/k_2)\right\} + D \end{cases} \tag{45}$$

When the system has uncertain disturbance $d(\mathrm{t})$, the PPSMRL can only guarantee that the sliding mode variables s and $\dot{s}$ converge to a region containing the origin in a finite time. $s = \dot{s} = 0$ cannot be guaranteed. Therefore, to use the second-order sliding mode property of the PPSMRL, the system uncertain disturbance $d(\mathrm{t})$ needs to be compensated. This problem will be studied in the next subsection.

B. DESIGN OF NON-HOMOGENEOUS DISTURBANCE OBSERVER

Consider the first-order single input single output (SISO) nonlinear system:

$$\dot{s} = d(\mathrm{t}) + u \tag{46}$$

where $s = 0$ defines the sliding surface, $u \in R$ is a system control input, and $d(\mathrm{t})$ is an uncertain function.

Designing a suitable input variable u can ensure that s and $\dot{s}$ converge to the origin within a finite time. From (46), it is seen that $\dot{s}$ is sensitive to the unknown disturbance $d(\mathrm{t})$. If s and u can be obtained in real-time, $d(\mathrm{t})$ is $m-1$ times differentiable, and $d^{(\mathrm{m}-1)}(\mathrm{t})$ has a known Lipschitz constant L.

Based on the non-homogeneous differentiator proposed by Levant in [38], this paper uses a NHDO to improve the steady-state accuracy [39]:

$$\begin{cases} \dot{z}_0 = v_0 + u \\ v_0 = h_0(z_0 - s) + z_1 \\ \dot{z}_1 = v_1 \\ v_1 = h_1(z_1 - v_0) + z_2 \\ \vdots \\ \dot{z}_{\mathrm{m}-1} = v_{\mathrm{m}-1} \\ v_{\mathrm{m}-1} = h_{\mathrm{m}-1}(z_{\mathrm{m}-1} - v_{\mathrm{m}-2}) + z_{\mathrm{m}} \\ \dot{z}_{\mathrm{m}} = h_{\mathrm{m}}(z_{\mathrm{m}} - v_{\mathrm{m}-1}) \end{cases} \tag{47}$$

where h_i is a function as follows:

$$h_i(s) = -\lambda_{m-i} L^{\frac{1}{m-i+1}} |s|^{\frac{m-i}{m-i+1}} \operatorname{sgn}(s) - \mu_{m-i} s \tag{48}$$

where $\mu_i > 0, i = 0, 1, \ldots, k$.

Assuming that $s(\mathrm{t})$ and $u(\mathrm{t})$ are measurable while λ_i and μ_i are sufficiently large in the reverse order, the following equation holds after experiencing a finite time transient process:

$$\begin{cases} z_0 = s(\mathrm{t}) \\ z_1 = d(\mathrm{t}) \\ \vdots \\ z_i = v_{i-1} = d^{(i-1)}, \end{cases} \quad i = 1, \ldots, m \tag{49}$$

Equations (47) and (48) hold in the Filippov sense. λ_i is chosen to provide for the finite-time convergence of the differentiator with $L \equiv 1$. The known standard values of the sequence λ_i are $\lambda_0 = 1.1, \lambda_1 = 1.5, \lambda_2 = 2, \lambda_3 = 3, \lambda_4 = 5$, and $\lambda_5 = 8$, which are sufficient for $m \le 5$ [38]. The standard values of the sequence μ_i can be chosen as $\mu_0 = 3$, $\mu_1 = 6$, $\mu_2 = 8$, $\mu_3 = 10$, $\mu_4 = 11$, and $\mu_5 = 12$.

C. SLIDING MODE WITH NON-HOMOGENEOUS DISTURBANCE OBSERVER

If the sliding mode dynamic is of (49) and $d(\mathrm{t})$ is smooth with a known Lipschitz constant $L > 0$ of $d^{(\mathrm{m}-1)}(\mathrm{t})$, u is taken as:

$$u = -k_1 fal(s, 1+\gamma, 1) - k_2 |s|^{1-\gamma} \operatorname{sgn}(s) - z_1 \tag{50}$$

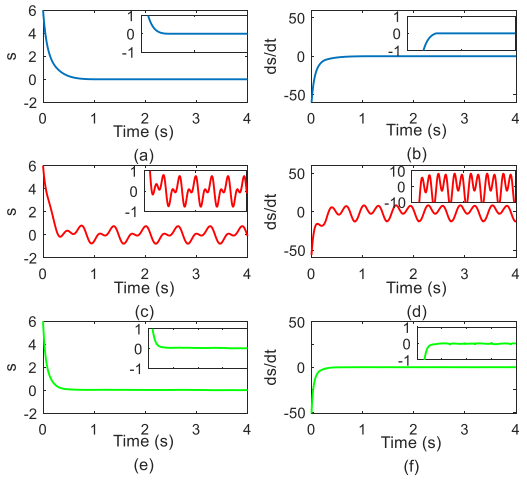

FIGURE 1. Three different system state conditions.

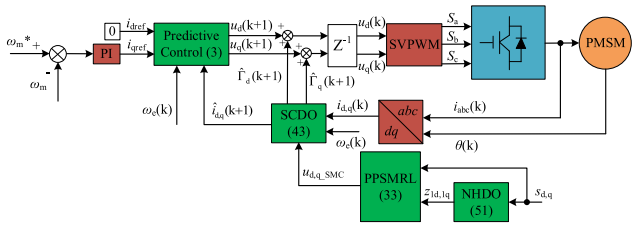

FIGURE 2. Block diagram of DPCC+SCDO+NHDO.

$$\begin{cases} \dot{z}_0 = v_0 + u \\ v_0 = -2L^{\frac{1}{3}}|z_0 - s|^{\frac{2}{3}}\,\mathrm{sgn}(z_0 - s) - 8(z_0 - s) + z_1 \\ \dot{z}_1 = v_1 \\ v_1 = -1.5L^{\frac{1}{2}}|z_1 - v_0|^{\frac{1}{2}}\,\mathrm{sgn}(z_1 - v_0) \\ \qquad\quad -6(z_1 - v_0) + z_2 \\ \dot{z}_2 = -1.1L\,\mathrm{sgn}(z_2 - v_1) - 3(z_2 - v_1) \end{cases} \tag{51}$$

where z_1 is the output of (51). According to (49), $z_1 = d(\mathrm{t})$ after a finite time transient process. The dynamic characteristics of the sliding mode at this time are consistent with (49). It can be seen that after a finite time, the sliding mode variables s and ds/dt converge to the origin, i.e., $s = \dot{s} = 0$.

Consider the following state disturbance:

$$d(\mathrm{t}) = 0.7\sin(2\mathrm{t}) + 0.5\cos\mathrm{t} \tag{52}$$

The state initial value is $s_0 = 6$, and the disturbance upper bound is $D = 10$. Fig. 1 verifies the discussions conducted above. The convergences of the system state s and ds/dt in the three cases are simulated. Figs. 1 (a) and (b) show the state convergences of s and ds/dt without any disturbance, which can go back to the origin in a limited time. Figs. 1 (c) and (d) show the s and ds/dt convergence to a bounded region as in (45) under a random disturbance, such as (52). Figs. 1 (e) and (f) are the simulation results with the proposed NHDO. It is seen that s and ds/dt can converge to the origin in a finite time under the disturbance. In conclusion,

TABLE 2. Parameters of the SPMSM.

Symbol	Quantity	Value
P	Number of pole pairs	4
R_s	Stator resistance (Ω)	0.365
L_d	Stator d-axis inductance (mH)	1.225
L_q	Stator q-axis inductance (mH)	1.225
ψ_f	Rotor flux linkage (Wb)	0.1667
J	Rotational inertia (kg·m^2)	0.00194

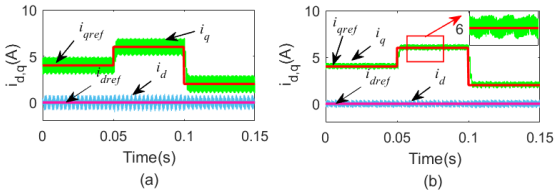

FIGURE 3. *d-q* axis current responses without parameter mismatch: (a) traditional DPCC; (b) improved DPCC.

with the proposed NHDO, more robust system is achieved under disturbance.

In conclusion, the discrete expression form of the DPCC+SCDO+NHDO can be written as:

$$\begin{cases} \boldsymbol{i}(\mathrm{k}+1) = \boldsymbol{A}(\mathrm{k})\boldsymbol{i}(\mathrm{k}) + \boldsymbol{C}\boldsymbol{u}(\mathrm{k}) + \boldsymbol{D}(\mathrm{k}) - \dfrac{T}{L}\hat{\boldsymbol{\Gamma}}(\mathrm{k}) \\ \qquad\qquad -\dfrac{T}{L}\hat{\boldsymbol{H}}(\mathrm{k}) \\ \boldsymbol{u}(\mathrm{k}+1) = \boldsymbol{C}^{-1}\left[\boldsymbol{i}(\mathrm{k}+2) - \boldsymbol{A}(\mathrm{k})\boldsymbol{i}(\mathrm{k}+1) - \boldsymbol{D}(\mathrm{k}+1)\right] \\ \hat{\boldsymbol{\Gamma}}(\mathrm{k}+1) = \hat{\boldsymbol{\Gamma}}(\mathrm{k}) - T\hat{\boldsymbol{H}}(\mathrm{k}) \\ \boldsymbol{U}^* = \boldsymbol{u}(\mathrm{k}) + \hat{\boldsymbol{\Gamma}}(\mathrm{k}+1) \end{cases} \tag{53}$$

where $\hat{\boldsymbol{H}}(\mathrm{k}) = \begin{bmatrix} u_{\mathrm{d\_SMC}}(\mathrm{k}) - z_{1\mathrm{d}}(\mathrm{k}) \\ u_{\mathrm{q\_SMC}}(\mathrm{k}) - z_{1\mathrm{q}}(\mathrm{k}) \end{bmatrix}$ represents the sliding mode reaching law including the compensation term for disturbance caused by SPMSM parameter mismatch

VI. SIMULATION

To evaluate the feasibility and efficiency of the proposed control method, simulation comparisons between the traditional DPCC and the improved DPCC algorithm are illustrated, and

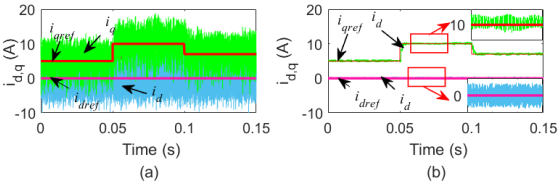

FIGURE 4. *d-q* axis current responses with L' = 4L: (a) traditional DPCC; (b) improved DPCC.

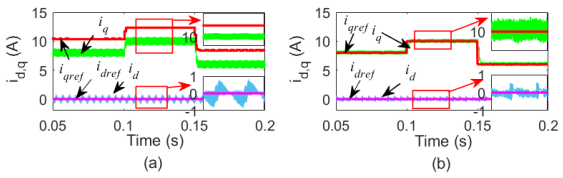

FIGURE 5. *d-q* axis current responses with $\Psi'_f = 0.5\Psi_f$: (a) traditional DPCC; (b) improved DPCC.

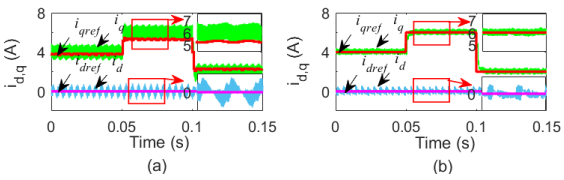

FIGURE 6. *d-q* axis current responses with $R'_s = 7R_s$: (a) traditional DPCC; (b) improved DPCC.

the simulation block diagram is shown in Fig. 2, and the motor parameters are listed in Table 2.

The inverter input DC voltage is 310 V, and the controller sampling time is 50 μs, while the deadtime is 2.5 μs. The parameters of the SCDO are $k_1 = 4000$, $k_2 = 2000$, and $\gamma = 0.5$, which are optimally selected based on simulation and experimental results. $\lambda_0 = 1.1$, $\lambda_1 = 1.5$, $\lambda_2 = 2$, $\mu_0 = 3$, $\mu_1 = 6$, and $\mu_2 = 8$ are parameters in the NHDO, they are fixed parameters and do not need to modify further [39].

In Fig. 3, the given mechanical speed is 900 r/min, and the load torque command is switched from 4 Nm to 6 Nm at 0.05 s and to 2 Nm at 0.1 s. i_{dref} and i_{qref} represent the referenced d- and q-axis currents, while i_d and i_q represent the real-time d- and q-axis currents, respectively. After the rotor speed reaches a steady state, the i_{qref} changes from 4 A to 6 A and 2 A. It is found that the current ripples in the improved

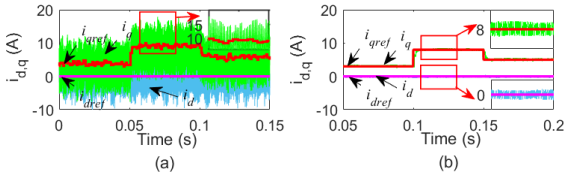

FIGURE 7. *d-q* axis current responses with $R'_s = 5R_s$, $L' = 4.5L$, $\Psi'_f = 1.5\Psi_f$: (a) traditional DPCC; (b) improved DPCC.

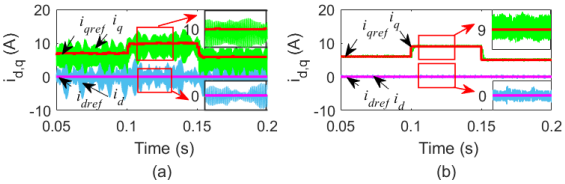

FIGURE 8. *d-q* axis current responses with $R'_s = 0.1R_s$, $L' = 2L$, $\Psi'_f = 0.8\Psi_f$: (a) traditional DPCC; (b) improved DPCC.

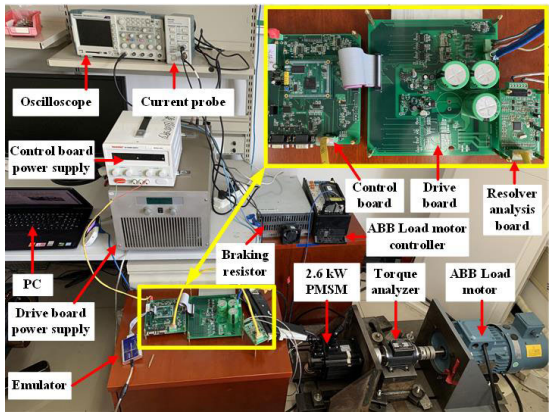

FIGURE 9. Experiment platform of the SPMSM system.

DPCC method, as shown in Fig. 3 (b), are lower than that in the traditional DPCC, as shown in Fig. 3 (a).

Fig. 4 demonstrates the current dynamic and steady responses when the inductance parameters mismatch, i.e., the estimated value of inductance L' is four times of real value L. The load torque command varies from 5 Nm to 10 Nm and 7 Nm with a rotor speed of 1000 r/min. In the traditional DPCC, the i_{qref} changes from 5 A to 10 A and 7 A. The d-q axis currents fail to accurately follow the reference currents and with large ripple, as shown in Fig. 4 (a). However, under the same operating condition, in the improved DPCC, d-q axis currents can change immediately according to the reference current and with lower ripples, as shown in Fig. 4 (b).

When the permanent magnet (PM) flux linkages mismatch, e.g., $\Psi'_f = 0.5\Psi_f$, the steady-state error of q-axis current is approximately zero in the improved DPCC, while that in the traditional DPCC is far away from zero, as shown in Fig. 5. Moreover, the current ripple in the improved DPCC is significantly smaller than that in the traditional DPCC. Similarly, superior performance can be obtained with the improved DPCC when the resistance mismatch, as shown in Fig. 6.

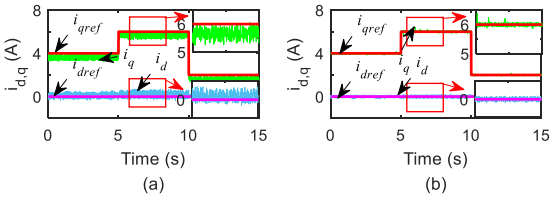

FIGURE 10. Experimental results of d-q axis current responses without parameter mismatch: (a) traditional DPCC; (b) improved DPCC.

When three major parameters mismatch, two cases are investigated in this study. In Fig. 7, the mismatched parameters are $R'_s = 5R_s$, $L' = 4.5L$, and $\Psi'_f = 1.5\Psi_f$. If the drive system is with the traditional DPCC, the d-q axis currents oscillate widely near the reference currents. Furthermore, the negative q-axis current appears, resulting in serious vibration, as shown in Fig. 7 (a). However, in the improved DPCC

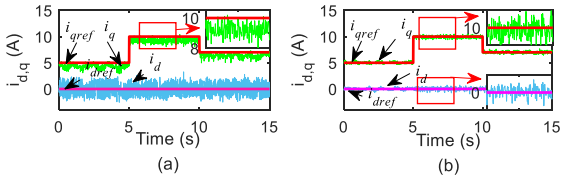

FIGURE 11. Experimental results of *d-q* axis current responses with $L' = 4L$: (a) traditional DPCC; (b) improved DPCC.

drive system, as shown in Fig. 7 (b), the performance of the d-q axis currents keeps accurate and has low ripples. In Fig. 8, with $R'_s = 0.1R_s$, $L' = 2L$, $\Psi'_f = 0.8\Psi_f$, more robust current responses are revealed in the improved DPCC drive system. The simulation results of six parameter mismatch situations suggest that, compared with the traditional DPCC, the improved DPCC can acquire better dynamic and static tracking characteristics.

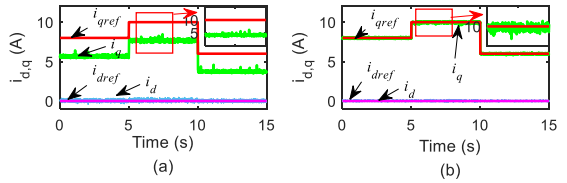

FIGURE 12. Experimental results of *d-q* axis current responses with $\Psi'_f = 0.5\Psi_f$: (a) traditional DPCC; (b) improved DPCC.

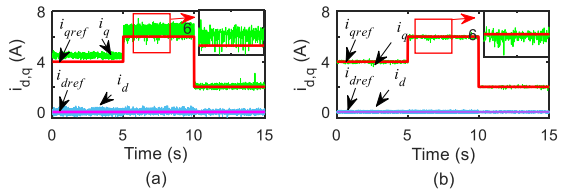

FIGURE 13. Experimental results of *d-q* axis current responses with $R'_s = 7R_s$: (a) traditional DPCC; (b) improved DPCC.

VII. EXPERIMENTS VERIFICATION

Both the traditional DPCC and the improved DPCC dive systems are experimentally tested under the same load conditions on the SPMSM experimental platform, as shown in Fig. 9. It mainly includes an SPMSM of 2.6 kW rated power, an ABB load motor, an inverter with a DC power supply (130 V), an oscilloscope, and a PC. The main control chip adopts TMS320F28377d. The controller sampling time is 50 μs, and the deadtime is 2.5 μs. The experimental conditions are consistent with the simulation conditions to verify the authenticity and validity of the simulation results. However, it is complicated to change the parameters of the motor in the experiment. The alternative method is changing the parameters of the motor in the control program to simulate the parameter mismatch.

Fig. 10 shows the tracking performance of *d-q* axis real-time currents without parameter mismatch at 900 r/min. Due to the non-linear characteristics of the actual control circuit

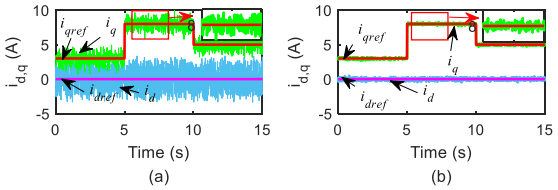

FIGURE 14. Experimental results of d-q axis current responses with $R'_s = 5R_s$, $L' = 4.5L$, $\Psi'_f = 1.5\Psi_f$: (a) traditional DPCC; (b) improved DPCC.

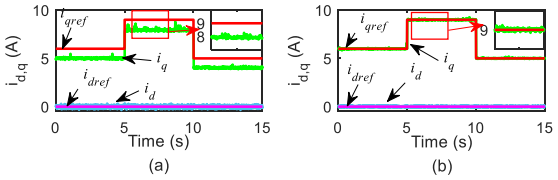

FIGURE 15. Experimental results of d-q axis current responses with $R'_s = 0.1R_s$, $L' = 2L$, $\Psi'_f = 0.8\Psi_f$: (a) traditional DPCC; (b) improved DPCC.

with the traditional DPCC, i_d and i_q deviate slightly from the reference values, as shown in Fig. 10 (a). Fig. 10 (b) depicts a better real-time current tracking performance in the same condition with the improved DPCC drive system.

Compared with the same condition of $L' = 4L$ in the simulation, experimental results are quite different due to the error between the theoretical model and the actual motor. In the traditional DPCC, i_d has large ripples, and i_q cannot accurately follow the reference current and produces irregular vibrations, as shown in Fig. 11 (a). The current oscillation caused by the inductance estimation mismatch can be vastly reduced with the improved DPCC algorithm, as shown in Fig. 11 (b).

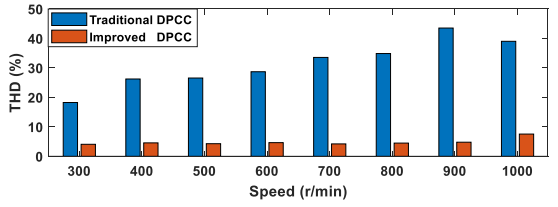

FIGURE 16. Experimental results of THD (%) of two methods under different motor speeds.

The experimental verification under the flux linkage mismatch is shown in Fig. 12. It can be seen that the experimental results are similar to the simulation in Fig. 5. The steady-state error of i_q in the improved DPCC is much smaller than that in the traditional DPCC, and the current ripples are also more minor, as shown in Fig. 12 (b). Similar results also occur in the experimental verification of the stator resistance mismatch, as shown in Fig. 13.

Figs. 14 and 15 demonstrate the two cases of three major parameters of the SPMSM mismatch. In Fig. 14, the same mismatched parameters with simulation are $R'_s = 5R_s$, $L' = 4.5L$, $\Psi'_f = 1.5\Psi_f$. The *d-q* axis currents fluctuate

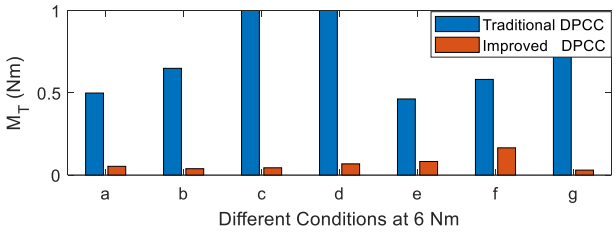

FIGURE 17. M_T (Nm) of two methods under different parameter mismatch conditions.

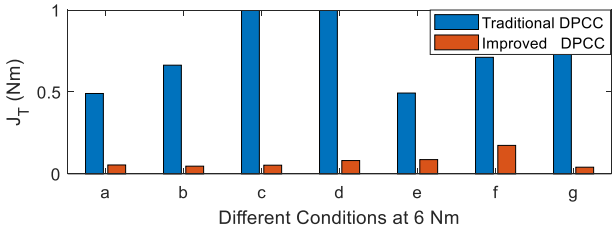

FIGURE 18. J_T (Nm) of two methods under different parameter mismatch conditions.

greatly near the reference value, especially the d-axis current fluctuation phenomenon is more severe in the traditional DPCC, as shown in Fig. 14 (a). The fluctuation caused by this parameter mismatch is reduced in the improved DPCC, as shown in Fig. 14 (b). However, in the case of another three parameters mismatch, $R'_s = 0.1R_s$, $L' = 2L$, $\Psi'_f = 0.8\Psi_f$ in Fig. 15, the d-axis current can be well maintained near 0 under both algorithms. The error between the q-axis current and the reference current is 1 A, as shown in Fig. 15 (a). The improved DPCC drive system revealed more robust current responses, as shown in Fig. 15 (b).

It is found that the experimental results look better than the simulation results. The reasons behind it may be that instruments and meters in the experiment contain signal processing and filtering functions, but there is no further filter and processing in the simulation model.

To further illustrate the effectiveness of the proposed method, Fig. 16 compares the total harmonic distortion (THD) of phase current of traditional DPCC and improved DPCC when inductance parameter mismatch. The THD of the traditional DPCC is much higher than that of the improved DPCC in the motor speed range from 300 r/min to 1000 r/min. More specifically, the maximum THD of the traditional DPCC exceeds 40 %, while that in the improved DPCC is less than 8 %.

To further evaluate the magnitude of motor torque pulsation under SPMSM parameter mismatch, two evaluation formulas (54) and (55) of torque pulsation evaluation [12] are used in this paper. The mechanical speed of SPMSM is 800 r/min, and the load torque is 6 Nm. Figs. 17 and 18 present the torque tracking performance under different conditions. It can be seen that the torque tracking accuracy in the improved DPCC is much better than that in the traditional DPCC. The above-mentioned parameter mismatch

TABLE 3. Different working conditions.

Symbol	Working conditions
a	Without parameter mismatch
b	$L' = 4L$
c	$\Psi'_f = 1.5\Psi_f$
d	$\Psi'_f = 0.5\Psi_f$
e	$R'_s = 7R_s$
f	$R'_s = 5R_s$, $L' = 4.5L$, $\Psi'_f = 1.5\Psi_f$
g	$R'_s = 0.1R_s$, $L' = 2L$, $\Psi'_f = 0.8\Psi_f$

conditions are listed in Table 3.

$$M_T = \frac{1}{N}\sum_{k=1}^{N}|e_T(k)| = \frac{1}{N}\sum_{k=1}^{N}\left|T^{ref}(k) - T(k)\right| \tag{54}$$

$$J_T = \sqrt{\frac{1}{N}\sum_{k=1}^{N}(e_T(k))^2} = \sqrt{\frac{1}{N}\sum_{k=1}^{N}\left(T^{ref}(k) - T(k)\right)^2} \tag{55}$$

Evidently, the above experiment and analysis results stated that in the case of motor parameter mismatch, the torque pulsation of improved DPCC can be dramatically reduced compared with the traditional DPCC.

VIII. CONCLUSION

This paper presented an improved DPCC with an enhanced disturbance observer to increase the robustness of the PMSM drive system. With the SCDO and NHDO, the d-q axis currents can be accurately observed, and the voltage compensation can be immediately output when there are disturbances, such as parameter mismatch. In the SCDO, the PPSMRL suppresses the sliding-mode chattering and accelerates the current error convergence rate. To further increase the robustness of the drive system, NHDO is proposed to observe and compensate for the disturbances to eliminate chattering.

Both simulations and experiments are explored to verify the superior performance of the improved DPCC. Whether parameter mismatch occurs, the current ripples and current harmonics in the traditional DPCC are more significant than those in the proposed DPCC. When parameter mismatch occurs with different situations, the output current of the traditional DPCC fails to follow the reference current accurately. Moreover, torque pulsation of the traditional DPCC is significant. In contrast, the current ripple, current harmonics, and torque pulsation in the proposed DPCC can be effectively suppressed. Once parameter mismatched, the robustness of the PMSM drive system in output current tracking performance can be enhanced remarkably.

REFERENCES

[1] M. P. Kazmierkowski and L. Malesani, "Current control techniques for three-phase voltage-source PWM converters: A survey," *IEEE Trans. Ind. Electron.*, vol. 45, no. 5, pp. 691–703, Oct. 1998.
[2] B. Sarsembayev, K. Suleimenov, and T. D. Do, "High order disturbance observer based PI-PI control system with tracking anti-windup technique for improvement of transient performance of PMSM," *IEEE Access*, vol. 9, pp. 66323–66334, 2021.

[3] Z. Zhang, L. Jing, X. Wu, W. Xu, J. Liu, G. Lyu, and Z. Fan, "A deadbeat PI controller with modified feedforward for PMSM under low carrier ratio," *IEEE Access*, vol. 9, pp. 63463–63474, 2021.

[4] X. Fu, H. He, Y. Xu, and X. Fu, "A strongly robust and easy-tuned current controller for PMSM considering parameters variation," *IEEE Access*, vol. 8, pp. 44228–44238, 2020.

[5] T. Li, R. Ma, and W. Han, "Virtual-vector-based model predictive current control of five-phase PMSM with stator current and concentrated disturbance observer," *IEEE Access*, vol. 8, pp. 212635–212646, 2020.

[6] X. Yuan, S. Zhang, and C. Zhang, "Enhanced robust deadbeat predictive current control for PMSM drives," *IEEE Access*, vol. 7, pp. 148218–148230, 2019.

[7] Y. Yao, Y. Huang, F. Peng, J. Dong, and H. Zhang, "An improved deadbeat predictive current control with online parameter identification for surface-mounted PMSMs," *IEEE Trans. Ind. Electron.*, vol. 67, no. 12, pp. 10145–10155, Dec. 2020.

[8] Y. Jiang, W. Xu, C. Mu, and Y. Liu, "Improved deadbeat predictive current control combined sliding mode strategy for PMSM drive system," *IEEE Trans. Veh. Technol.*, vol. 67, no. 1, pp. 251–263, Jan. 2018.

[9] X. Ba, P. Wang, C. Zhang, J. G. Zhu, and Y. Guo, "Improved deadbeat predictive current control to enhance the performance of the drive system of permanent magnet synchronous motors," *IEEE Trans. Appl. Supercond.*, vol. 31, no. 8, pp. 1–4, Nov. 2021.

[10] W. Song, J. Ma, L. Zhou, and X. Feng, "Deadbeat predictive power control of single-phase three-level neutral-point-clamped converters using space-vector modulation for electric railway traction," *IEEE Trans. Power Electron.*, vol. 31, no. 1, pp. 721–732, Jan. 2016.

[11] S. Li and Z. Liu, "Adaptive speed control for permanent-magnet synchronous motor system with variations of load inertia," *IEEE Trans. Ind. Electron.*, vol. 56, no. 8, pp. 3050–3059, Aug. 2009.

[12] J. Gao, C. Gong, W. Li, and J. Liu, "Novel compensation strategy for calculation delay of finite control set model predictive current control in PMSM," *IEEE Trans. Ind. Electron.*, vol. 67, no. 7, pp. 5816–5819, Jul. 2020.

[13] M. F. Elmorshedy, W. Xu, F. F. M. El-Sousy, M. Rabiul Islam, and A. A. Ahmed, "Recent achievements in model predictive control techniques for industrial motor: A comprehensive state-of-the-art," *IEEE Access*, vol. 9, pp. 58170–58191, 2021.

[14] Y. Yang, H. Wen, and D. Li, "A fast and fixed switching frequency model predictive control with delay compensation for three-phase inverters," *IEEE Access*, vol. 5, pp. 17904–17913, 2017.

[15] R. Shah and R. Gajjar, "A comparative study of various methods for parameter estimation of PMSM," in *Proc. Int. Conf. Energy, Commun., Data Anal. Soft Comput. (ICECDS)*, Chennai, India, Aug. 2017, pp. 1712–1715.

[16] X. Li, S. Zhang, C. Zhang, Y. Zhou, and C. Zhang, "An improved deadbeat predictive current control scheme for open-winding permanent magnet synchronous motors drives with disturbance observer," *IEEE Trans. Power Electron.*, vol. 36, no. 4, pp. 4622–4632, Apr. 2021.

[17] F. Wang and L. He, "FPGA-based predictive speed control for PMSM system using integral sliding-mode disturbance observer," *IEEE Trans. Ind. Electron.*, vol. 68, no. 2, pp. 972–981, Feb. 2021.

[18] L. Yan, F. Wang, M. Dou, Z. Zhang, R. Kennel, and J. Rodriguez, "Active disturbance-rejection-based speed control in model predictive control for induction machines," *IEEE Trans. Ind. Electron.*, vol. 67, no. 4, pp. 2574–2584, Apr. 2020.

[19] H. Yang, Y. Zhang, J. Liang, J. Liu, N. Zhang, and P. D. Walker, "Robust deadbeat predictive power control with a discrete-time disturbance observer for PWM rectifiers under unbalanced grid conditions," *IEEE Trans. Power Electron.*, vol. 34, no. 1, pp. 287–300, Jan. 2019.

[20] S. Niu, Y. Luo, W. Fu, and X. Zhang, "Robust model predictive control for a three-phase PMSM motor with improved control precision," *IEEE Trans. Ind. Electron.*, vol. 68, no. 1, pp. 838–849, Jan. 2021.

[21] X. Zhang, B. Hou, and Y. Mei, "Deadbeat predictive current control of permanent-magnet synchronous motors with stator current and disturbance observer," *IEEE Trans. Power Electron.*, vol. 32, no. 5, pp. 3818–3834, May 2017.

[22] X. Chang and G. Yang, "Nonfragile H_∞ filter design for T–S fuzzy systems in standard form," *IEEE Trans. Ind. Electron.*, vol. 61, no. 7, pp. 3448–3458, Jul. 2014.

[23] Z. Li and X. Chang, "Robust H_∞ control for networked control systems with randomly occurring uncertainties: Observer-based case," *ISA Trans.*, vol. 83, pp. 13–24, Dec. 2018.

[24] Q. Hou and S. Ding, "GPIO based super-twisting sliding mode control for PMSM," *IEEE Trans. Circuits Syst. II, Exp. Briefs*, vol. 68, no. 2, pp. 747–751, Feb. 2021.

[25] L. Liu, S. Ding, and X. Yu, "Second-order sliding mode control design subject to an asymmetric output constraint," *IEEE Trans. Circuits Syst. II, Exp. Briefs*, vol. 68, no. 4, pp. 1278–1282, Apr. 2021.

[26] A. K. Junejo, W. Xu, C. Mu, M. M. Ismail, and Y. Liu, "Adaptive speed control of PMSM drive system based a new sliding-mode reaching law," *IEEE Trans. Power Electron.*, vol. 35, no. 11, pp. 12110–12121, Nov. 2020.

[27] P. Gao, G. Zhang, H. Ouyang, and L. Mei, "An adaptive super twisting nonlinear fractional order PID sliding mode control of permanent magnet synchronous motor speed regulation system based on extended state observer," *IEEE Access*, vol. 8, pp. 53498–53510, 2020.

[28] Q. Wang, H. Yu, M. Wang, and X. Qi, "An improved sliding mode control using disturbance torque observer for permanent magnet synchronous motor," *IEEE Access*, vol. 7, pp. 36691–36701, 2019.

[29] Y. Yang, Z. Long, and Y. Xie, "An improved sliding mode control via discrete time optimal control and its application to magnetic suspension system," *IEEE Access*, vol. 8, pp. 185584–185594, 2020.

[30] W. Xu, A. K. Junejo, Y. Liu, M. G. Hussien, and J. Zhu, "An efficient antidisturbance sliding-mode speed control method for PMSM drive systems," *IEEE Trans. Power Electron.*, vol. 36, no. 6, pp. 6879–6891, Jun. 2021.

[31] L. Yipeng, L. Jie, Z. Fengge, and Z. Ming, "Fuzzy sliding mode control of magnetic levitation system of controllable excitation linear synchronous motor," *IEEE Trans. Ind. Appl.*, vol. 56, no. 5, pp. 5585–5592, Sep. 2020.

[32] W. Gao, *Theory and Design Method for Variable Sliding Mode Control*. Beijing, China: Science Press, 1996, pp. 28–29.

[33] P. Li, J. Ma, and Z. Zheng, "Sliding mode control approach based on nonlinear integrator," *IET Control Theory Appl.*, vol. 28, no. 5, pp. 619–624, 2011.

[34] S. Yu, X. Yu, B. Shirinzadeh, and Z. Man, "Continuous finite-time control for robotic manipulators with terminal sliding mode," *Automatica*, vol. 41, no. 11, pp. 1957–1964, Nov. 2005.

[35] L. Yang and J. Yang, "Nonsingular fast terminal sliding-mode control for nonlinear dynamical systems," *Int. J. Robust Nonlinear Control*, vol. 21, no. 16, pp. 1865–1879, Nov. 2011.

[36] F. W. Olver, D. Lozier, and R. F. Boisvert, *NIST Handbook of Mathematical Functions*. Cambridge, U.K.: Cambridge Univ. Press, 2010, pp. 713–715.

[37] Y. Liao, Y. Yang, and Y. Wang, "Novel double power combination function reaching law for sliding mode control," *J. Nat. Univ. Defense Technol.*, vol. 39, no. 3, pp. 105–110, 2017.

[38] A. Levant, "Non-homogeneous finite-time-convergent differentiator," in *Proc. 48h IEEE Conf. Decis. Control (CDC) held Jointly 28th Chin. Control Conf.*, Shanghai, China, Dec. 2009, pp. 8399–8404.

[39] P. Li, P. Wang, J. Ma, and X. Peng, "Non-homogeneous disturbance observer-based second order sliding mode control," in *Proc. 33rd Chin. Control Conf.*, Naijing, China, Jul. 2014, pp. 2150–2154.

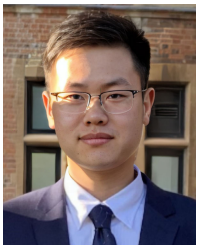

ZHENJIE GONG was born in Inner Mongolia, China, in 1992. He received the B.E. degree in automation from the Inner Mongolia University of Technology, China, in 2014, and the M.E. degree in electrical engineering from Beijing Information Science and Technology University, China, in 2018. He is currently pursuing the Ph.D. degree with the National Engineering Laboratory for Electric Vehicles, School of Mechanical Engineering, Beijing Institute of Technology.

His research interests include study on high precision of synchronous motor, and power electronic drives and control.

CHENGNING ZHANG received the M.E. degree in control theory and control engineering and the Ph.D. degree in vehicle engineering from the Beijing Institute of Technology, Beijing, China, in 1989 and 2001, respectively.

He is currently a Professor with the National Engineering Laboratory for Electric Vehicles, Beijing Institute of Technology. His research interests include electric vehicles, vehicular electric motor drive systems, battery management systems, and chargers.

XIN BA received the B.E. degree from the Lanzhou University of Technology, Lanzhou, China, in 2011, the M.E. degree from Beijing Information Science and Technology University, Beijing, China, in 2015, and the Ph.D. degree from the Beijing Institute of Technology, China, in 2020, all in mechanical engineering. She is currently pursuing the Ph.D. degree in electrical engineering with the School of Electrical and Data Engineering, University of Technology Sydney, Australia.

She is also a Postdoctoral Fellow with the School of Mechanical Engineering, Beijing Institute of Technology. Her research interests include measurement and modeling of properties of magnetic materials, and numerical analysis of electromagnetic field.

YOUGUANG GUO (Senior Member, IEEE) received the B.E. degree from the Huazhong University of Science and Technology, China, in 1985, the M.E. degree from Zhejiang University, China, in 1988, and the Ph.D. degree from the University of Technology Sydney (UTS), Australia, in 2004, all in electrical engineering.

He is currently a Professor in electrical engineering with the School of Electrical and Data Engineering, UTS. His research interests include measurement and modeling of properties of magnetic materials, numerical analysis of electromagnetic field, electrical machine design optimization, and power electronic drives and control.